ELSEVIER

Volume 183, Issue 6, June 2010

JOURNAL OF SOLID STATE CHEMISTRY

www.elsevier.com/locate/jssc

CONTENTS

Abstracted/indexed in BioEngineering Abstracts, Chemical Abstracts, Coal Abstracts, Current Contents/Physics, Chemical, & Earth Sciences, Engineering Index, Research Alert, SCISEARCH, Science Abstracts, and Science Citation Index. Also covered in the abstract and citation database SCOPUS®. Full text available on ScienceDirect®.

Regular Articles

Sol–gel synthesis of mesoporous $CaCu_3Ti_4O_{12}$ thin films and their gas sensing response
R. Parra, R. Savu, L.A. Ramajo, M.A. Ponce, J.A. Varela, M.S. Castro, P.R. Bueno and E. Joanni
Page 1209

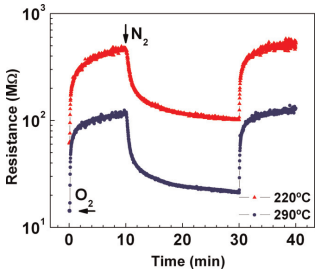

A sol–gel synthesis procedure toward stable $CaCu_3Ti_4O_{12}$-precursor sols avoiding the precipitation of undesired compounds is proposed. Films deposited by spin-coating onto oxidized silicon substrates were annealed at 700 °C. The thickness varied between 200 and 400 nm depending on sol composition. The films, tested as gas sensors for O_2, showed n-type conductivity, good sensitivity and short response times.

$Ca_4Fe_{3-x}Mn_xO_{8-\delta}Cl_2$: A new $n=3$ Ruddlesden–Popper oxychloride
Tao Yang, Junliang Sun, Mark Croft, Israel Nowik, Alexander Ignatov, Rihong Cong and Martha Greenblatt
Page 1215

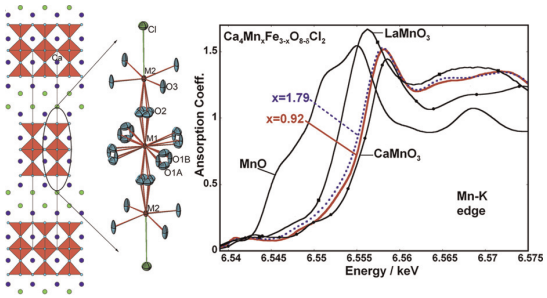

Structural analysis by the X-ray diffraction, the ^{57}Fe Mössbauer and the X-ray absorption spectroscopy shows that all Fe ions are trivalent, the valence of Mn varies from ~4+ to 3+/4+ with increasing x.

Regular Articles—Continued

$K_2Fe_2B_2O_7$: A transparent nonlinear optical crystal with frustrated magnetism
Yonggang Wang and R.K. Li
Page 1221

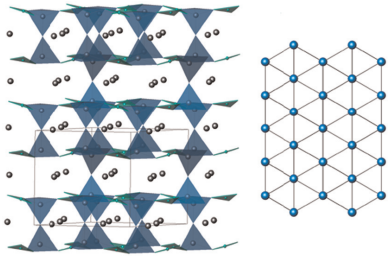

Single crystal of a new ferroborate $K_2Fe_2B_2O_7$, space group $P321$, $a=8.7475(3)$ Å, $c=8.5124(3)$ Å, was obtained and characterized. It exhibits considerable SHG efficiency and frustrated magnetism originated from the triangular Fe net in the ab plane.

A novel $4^4.6^6$ 5-connected metal-organic framework with strong fluorescent emission constructed by *m*-thioacetatebenzoic acid
Cai-Hong Zhan and Yun-Long Feng
Page 1226

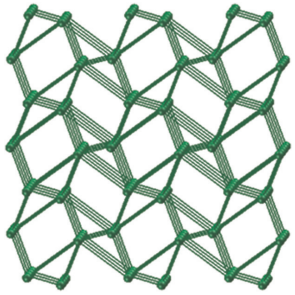

A novel 5-connected nov ($4^4.6^6$) topology network, $[Cd_2L_2(4,4'\text{-bipy})_{3/2}(H_2O)_2]_n$ (H_2L = *m*-thioacetatebenzoic acid and 4,4′-bipy = 4,4′-bipyridine), was prepared under hydrothermal condition and it displays intense structure-related fluorescent emission.

Continued

Structure and conductivity of strontium-doped cerium orthovanadates $Ce_{1-x}Sr_xVO_4$ ($0 \le x \le 0.175$)
Christophe T.G. Petit, Rong Lan, Peter I. Cowin and Shanwen Tao
Page 1231

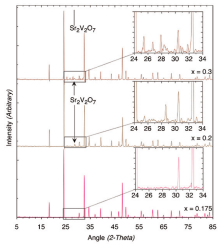

A-site substituted cerium orthovanadates $Ce_{1-x}Sr_xVO_4$ were synthesised by solid state reaction and their conductivities measured in air and dry 5% H_2/Ar up to the strontium solid solution limit.

One-dimensional NiCuZn ferrite nanostructures: Fabrication, structure, and magnetic properties
Jun Xiang, Xiangqian Shen, Fuzhan Song and Mingquan Liu
Page 1239

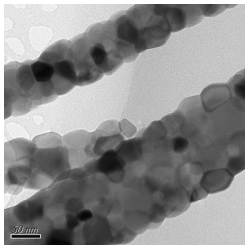

NiCuZn ferrite nanofibers with diameters of 80–160 nm have been prepared by electrospinning technique and their magnetic behavior is different from that of the corresponding powder sample.

Low temperature structural variations and molar heat capacity of stolzite, $PbWO_4$
Dmytro M. Trots, Anatoliy Senyshyn and Björn C. Schwarz
Page 1245

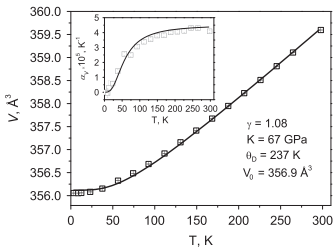

The thermal evolution of the $PbWO_4$ volume parameterized in the framework of a 1st order Grüneisen approximation using the Debye model for the internal energy:

$$V(T) = V_0 + \frac{\gamma}{K}U(T) \quad (1)$$

Improvement of the thermoelectric properties of $[Bi_{1.68}Ca_2O_{4-\delta}]^{RS}[CoO_2]_{1.69}$ cobaltite by chimie douce methods
Hervé Muguerra, Beatriz Rivas-Murias, Maria Traianidis, Catherine Henrist, Bénédicte Vertruyen and Rudi Cloots
Page 1252

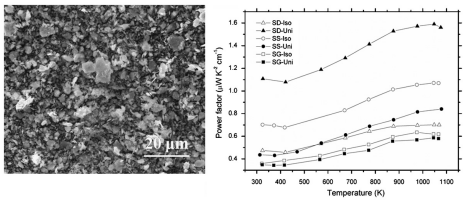

Small particles and narrow size distribution is obtained for spray-drying $[Bi_{1.68}Ca_2O_4]^{RS}[CoO_2]_{1.69}$ cobaltate. The power factor is boosted up two times compared with the conventional solid state method.

Synthesis and structural characterization of $A_3In_2Ge_4$ and $A_5In_3Ge_6$ (A = Ca, Sr, Eu, Yb)—New intermetallic compounds with complex structures, exhibiting Ge–Ge and In–In bonding
Tae-Soo You and Svilen Bobev
Page 1258

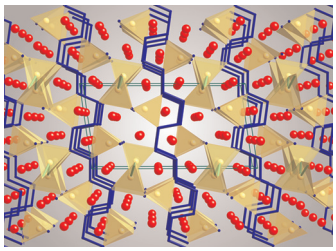

The anion sub-network of $A_5In_3Ge_6$ is based upon tetrahedral [$InGe_4$] chains, Ge_4 tetramers isosteric with 1,3-*cis*-butadiene, and distorted square-planar [$InGe_4$] fragments. The structure of $A_3In_2Ge_4$ is a combination of infinite Ge chains with *cis*- and *trans*-bonds in a complex $(tttctc)_n$ pattern, tetrahedral [$InGe_4$] chains, and In zig-zag chains.

Thermodynamics of $CoAl_2O_4$–$CoGa_2O_4$ solid solutions
Kristina I. Lilova, Alexandra Navrotsky, Brent C. Melot and Ram Seshadri
Page 1266

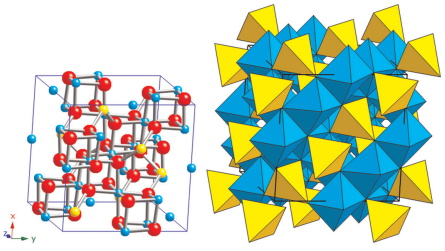

Measured enthalpies of mixing of $CoAl_2O_4$–$CoGa_2O_4$ solid solutions are close to zero but entropies of mixing reflect the complex cation distribution, so the system is not an ideal solution.

Structure and thermal conductivity of $Na_{1-x}Ge_{3+z}$
M. Beekman, S. Stefanoski, W. Wong-Ng, J.A. Kaduk, Q. Huang, C. Reeg, C.R. Bowers and G.S. Nolas
Page 1272

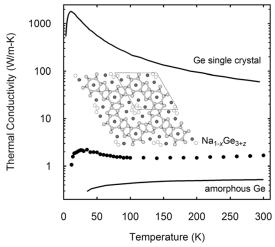

A zeolite-like intermetallic, $Na_{1-x}Ge_{3+z}$, is prepared by thermal decomposition of Na_4Ge_4. This binary phase exhibits an unusual crystal structure in which germanium forms large tunnels with significant disorder, and is found to possess a very low lattice thermal conductivity.

X-ray structural study of intermetallic alloys RT_2Si and $RTSi_2$ (R = rare earth, T = noble metal)
Alexander Gribanov, Andriy Grytsiv, Peter Rogl, Yurii Seropegin and Gerald Giester
Page 1278

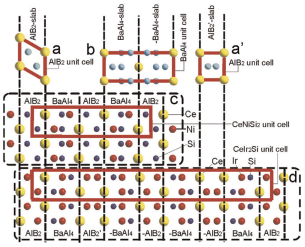

Two series of the intermetallic compounds, RT_2Si and $RTSi_2$, have been investigated by X-ray diffraction methods. The new tetragonal $CeIr_2Si$-type of the crystal structure was described and the interrelation between orthorhombic $CeNiSi_2$ and tetragonal $CeIr_2Si$ had been discussed as a similar packing of the $BaAl_4$ and AlB_2 slabs.

Ab-initio calculation of structural, electronic, and optical characterizations of the intermetallic trialuminides $ScAl_3$ compound
Ali Hussain Reshak, Z. Charifi and H. Baaziz
Page 1290

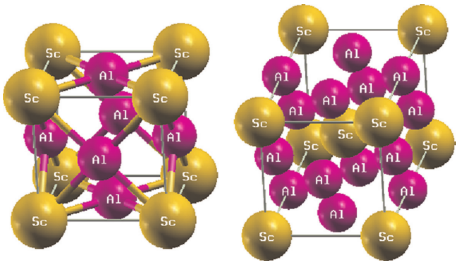

Crystal structure of $L1_2$ (a) and $D0_{22}$ (b) phases of $ScAl_3$ compound.

Structure determination of α-$La_6W_2O_{15}$
M.-H. Chambrier, R.M. Ibberson and F. Goutenoire
Page 1297

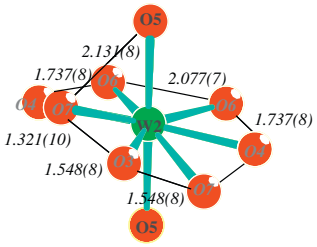

Projection of the polyhedra around the tungsten atom. Atoms labelled in grey are occupied at 50%. Short oxygen–oxygen distances are marked. The polyhedra represents $WO_{5.5}$ that is related to the structural unit W_2O_{11} unit. Alpha-$La_6W_2O_{15}$ could be described as $[O_2La_3]_2[WO_{5.5}]_2$.

Sensitized red luminescence from Ce^{3+}, Mn^{2+}-doped glaserite-type alkaline-earth silicates
Yoshinori Yonesaki, Takahiro Takei, Nobuhiro Kumada and Nobukazu Kinomura
Page 1303

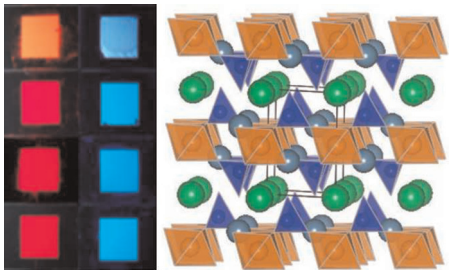

Glaserite-type red emitting phosphor, $M_2BaMgSi_2O_8$: Ce^{3+}, Mn^{2+} (M: Ba, Sr, Ca), was prepared by solid state reaction. Under UV excitation, Mn^{2+}-derived red emission is observed from the compounds only when Ce^{3+} ions are codoped, indicating that the red emission is caused by an energy transfer from Ce^{3+} to Mn^{2+}.

Crystal structure investigations of $ZrAs_xSe_y$ ($x > y$, $x + y \leq 2$) by single crystal neutron diffraction at 300 K, 25 K and 2.3 K
Rainer Niewa, Andreas Czulucki, Marcus Schmidt, Gudrun Auffermann, Tomasz Cichorek, Martin Meven, Björn Pedersen, Frank Steglich and Rüdiger Kniep
Page 1309

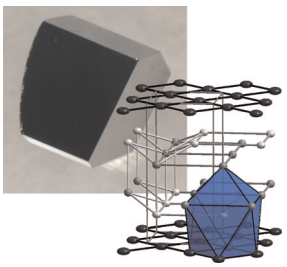

Large single crystals of $ZrAs_xSe_y$ grown by Chemical Transport to study structural details as the As–Se order scheme by single crystal neutron diffraction.

Continued

Magnetic properties of Fe_2P-type R_6CoTe_2 compounds (R = Gd–Er)
A.V. Morozkin, Yu Mozharivskyj, V. Svitlyk, R. Nirmala, O. Isnard, P. Manfrinetti, A. Provino and C. Ritter
Page 1314

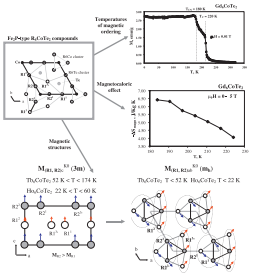

The novel Fe_2P-type R_6CoTe_2 phases (R = Gd–Er, space group $P\bar{6}2m$) show ferromagnetic type ordering in the temperature range 14–220 K.All compounds demonstrate high-temperature ferromagnetic and low-temperature antiferromagnetic ordering.The magnetic entropy of Gd_6CoTe_2 increases from $\Delta S_{mag} = -4.5$ J/kg K at 220 K up to $\Delta S_{mag} = -6.5$ J/kg K at 180 K for the field change $\Delta\mu_0 H = 0$–5 T.The R_6CoTe_2 compounds exhibit the commensurate magnetic structures with wave vectors $\mathbf{K}_0 = [0, 0, 0]$ and $\mathbf{K}_1 = [1/2, 1/2, 1/2]$.

Highly ordered Ti-SBA-15: Efficient H_2 adsorbent and photocatalyst for eco-toxic dye degradation
Swapan K. Das, Manas K. Bhunia and Asim Bhaumik
Page 1326

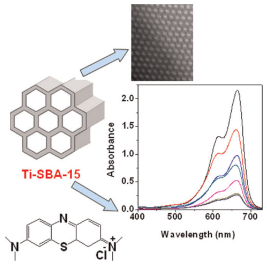

Highly ordered 2D-hexagonal mesoporous Ti-SBA-15 materials are synthesized hydrothermally, which show high H_2 adsorption capacity and excellent activity in the photocatalytic degradation of ecologically abundant dye methylene blue.

Synthesis, crystal structure, and structural conversion of Ni molybdate hydrate $NiMoO_4 \cdot nH_2O$
Kazuo Eda, Yasuyuki Kato, Yu Ohshiro, Takamitu Sugitani and M. Stanley Whittingham
Page 1334

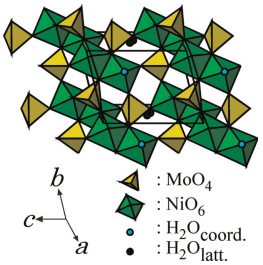

$NiMoO_4 \ldots nH_2O$ crystallized in the triclinic system with space group P-1, and its ideal chemical composition was $NiMoO_4 \ldots 3/4H_2O$ rather than $NiMoO_4 \ldots 1H_2O$.

One-dimensional CoPt nanorods and their anomalous IR optical properties
X.W. Zhou, R.H. Zhang, D.M. Zeng and S.G. Sun
Page 1340

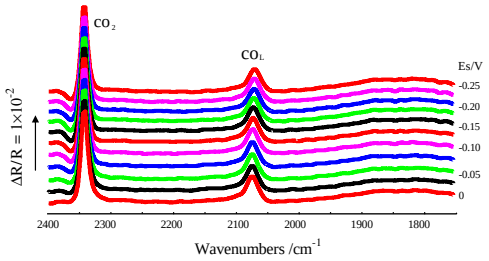

It has revealed, for the first time, that the 1D CoPt nanorods present abnormal infrared effects (AIREs). The substrate materials do not affect significantly the anomalous IR features.

Synthesis and characterization of $La_{1+x}Sr_{2-x}CoMnO_{7-\delta}$ (x = 0,0.2; δ = 0,1)
H. El Shinawi, A. Bertha, J. Hadermann, T. Herranz, B. Santos, J.F. Marco, F.J. Berry and C. Greaves
Page 1347

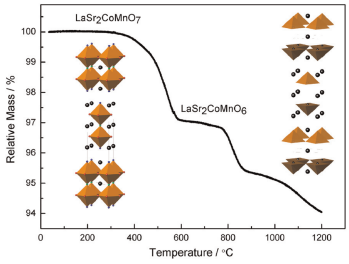

The $n = 2$ Ruddlesden–Popper phases $LaSr_2CoMnO_7$, $La_{1.2}Sr_{1.8}CoMnO_7$, $LaSr_2CoMnO_6$ and $La_{1.2}Sr_{1.8}CoMnO_6$ are synthesized and characterized.

Liquid–liquid interface assisted synthesis of size- and thickness-controlled Ag nanoplates
Ming-Shang Jin, Qin Kuang, Xi-Guang Han, Shui-Fen Xie, Zhao-Xiong Xie and Lan-Sun Zheng
Page 1354

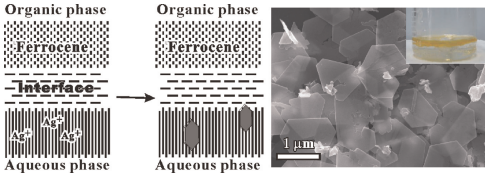

High-purity Ag nanoplates were synthesized by the reduction of aqueous Ag^+ ions at the aqueous–organic interface with the reductant ferrocene, the size and thickness of which were widely tunable.

Photo-degradation of methylene blue using Ta-doped ZnO nanoparticle
Ji-Zhou Kong, Ai-Dong Li, Xiang-Yu Li, Hai-Fa Zhai, Wen-Qi Zhang, You-Pin Gong, Hui Li and Di Wu
Page 1359

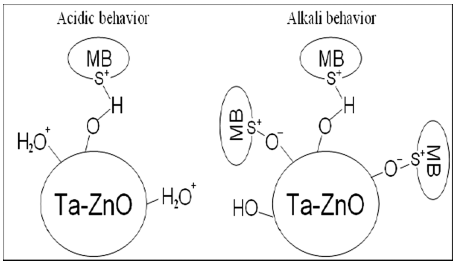

This model describes the adsorption between the amphoteric behavior of the metal oxide and the cationic dye methylene blue (MB) on the surface of the catalyst at the acidic and alkaline condition.

Preparation of three-dimensionally ordered macroporous perovskite-type lanthanum–iron-oxide $LaFeO_3$ with tunable pore diameters: High porosity and photonic property
Masahiro Sadakane, Toshitaka Horiuchi, Nobuyasu Kato, Keisuke Sasaki and Wataru Ueda
Page 1365

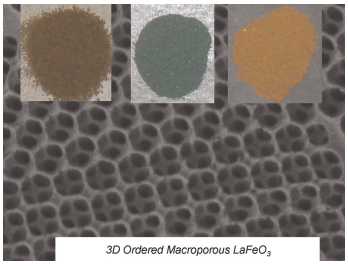

Well-ordered three-dimensionally ordered macroporous $LaFeO_3$ materials with pore sizes ranging from 127 to 321 nm were obtained in a high pore fraction.

Stabilization of over-stoichiometric Mn^{4+} in layered $Na_{2/3}MnO_2$
R. Stoyanova, D. Carlier, M. Sendova-Vassileva, M. Yoncheva, E. Zhecheva, D. Nihtianova and C. Delmas
Page 1372

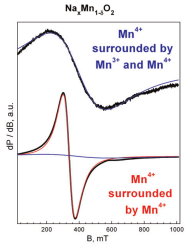

The composition and structure of $Na_{2/3}MnO_2$ were controlled by the rate of cooling from the temperature of preparation. By quenching from 1000 °C, the orthorhombic distorted modification is stabilized. A phase separation into orthorhombic and hexagonal modifications takes place when $Na_{2/3}MnO_2$ is slow cooled. The over-stoichiometric Mn^{4+} ions are accommodated in the hexagonal modification by creation of vacancies in the MnO_2-layers.

Dielectric properties of some $MM'O_4$ and $MTiM'O_6$ (M = Cr, Fe, Ga; M' = Nb, Ta, Sb) rutile-type oxides
Rohini Mani, S.N. Achary, Keka R. Chakraborty, S.K. Deshpande, Joby E. Joy, Abanti Nag, J. Gopalakrishnan and A.K. Tyagi
Page 1380

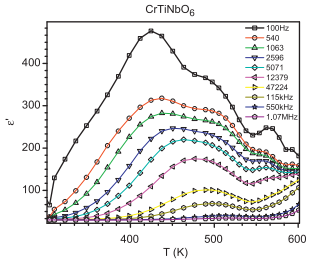

Dielectric response of $FeTiNbO_6$.

Lattice crossover and mixed valency in the $LaCo_{1-x}Rh_xO_3$ solid solution
Jun Li, Andrew E. Smith, Kyei-Sing Kwong, Cynthia Powell, Arthur W. Sleight and M.A. Subramanian
Page 1388

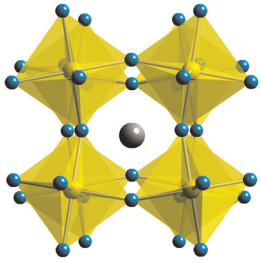

A complete solid solution is formed between $LaCoO_3$ and $LaRhO_3$. The effect of Rh substitution for Co on the lattice crossover, mixed valency and physical properties is described.

Synthesis and photocatalytic activity of co-doped mesoporous TiO_2 on Brij98/CTAB composite surfactant template
Xiaotong Zhang, Guowei Zhou, Jing Xu, Guangwei Bai and Lei Wang
Page 1394

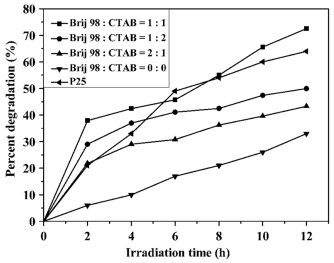

$CODc_r$ percent degradation of papermaking wastewater is about 73% after 12 h over the co-doped mesoporous TiO_2 prepared with a molar ratio of Brij98:CTAB = 1:1.

Continued

Consequence of doping mediated strain and the activation energy on the structural and optical properties of ZnO:Cr nanoparticles

Richa Bhargava, Prashant K. Sharma, Sanjeev Kumar, Avinash C. Pandey and Naresh Kumar

Page 1400

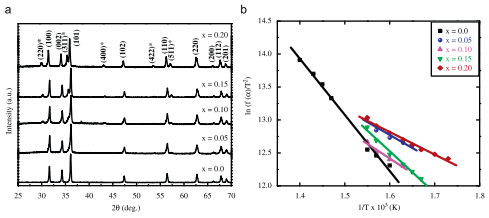

Cr-doped ZnO nanostructures were synthesized by sol–gel. XRD (a) revealed secondary phase of $ZnCr_2O_4$ with increase in Cr concentration. The Cr concentration also changes activation energy of the reaction (b).

Controllable preparation and fluorescence properties of Y^{3+} and Eu^{3+} co-doped mesoporous silica

Chao Zhang, Shanyi Guang and Hongyao Xu

Page 1409

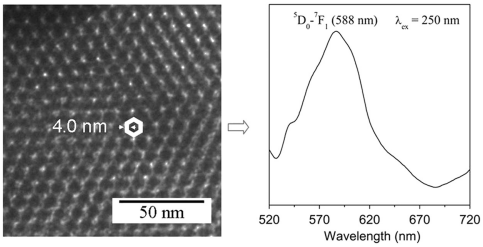

The Y^{3+} and Eu^{3+} co-doped well-ordered mesoporous silica through direct incorporation of rare-earth ions into wall of mesoporous materials show a widened emission band.

MAS-NMR investigations of the crystallization behaviour of lithium aluminum silicate (LAS) glasses containing P_2O_5 and TiO_2 nucleants

A. Ananthanarayanan, G.P. Kothiyal, L. Montagne and B. Revel

Page 1416

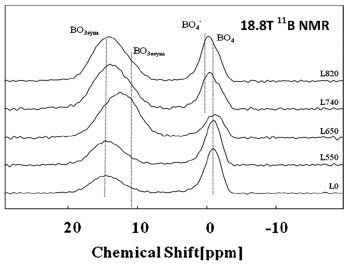

^{11}B MAS-NMR spectra of LAS glass heat treated at different temperatures, showing the evolution of the residual glass matrix during the crystallization treatment. High-field (18.8 T) NMR enables us to record high resolution spectra, from which the glass network modifications could be related to the formation of intermediate lithium silicate crystalline phases.

Template-free synthesis of CdS hollow nanospheres based on an ionic liquid assisted hydrothermal process and their application in photocatalysis

Xinping Li, Yanan Gao, Li Yu and Liqiang Zheng

Page 1423

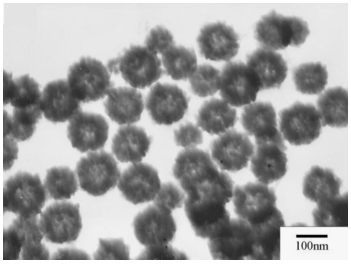

TEM images of typical as-prepared CdS hollow nanospheres.

Polytypic transformations during the thermal decomposition of cobalt hydroxide and cobalt hydroxynitrate

Thimmasandra Narayan Ramesh

Page 1433

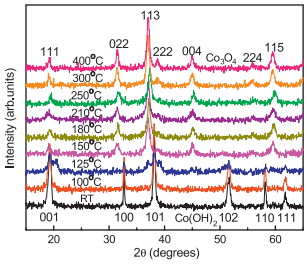

Isothermal thermal decomposition studies of cobalt hydroxide and cobalt hydroxynitrate at different intervals of temperature show the metastable phase formed prior to Co_3O_4 phase.

Preparation and photoluminescence properties of RE:$Na_3La_9O_3(BO_3)_8$ (RE = Er, Yb) crystals

Zuoliang Liu, Guochun Zhang, Jianxiu Zhang, Xiaoyan Bai, Peizhen Fu and Yicheng Wu

Page 1437

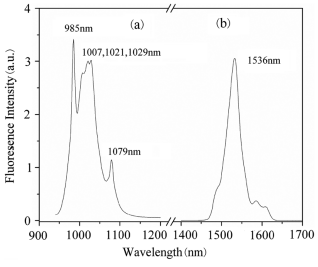

Fluorescence spectra show the emission peaks at 985, 1028 and 1079 nm of Yb:NLBO and at 1536 nm of Er:NLBO.

Solid state synthesis of water-dispersible silicon nanoparticles from silica nanoparticles
Keren Kravitz, Alexander Kamyshny, Aharon Gedanken and Shlomo Magdassi
Page 1442

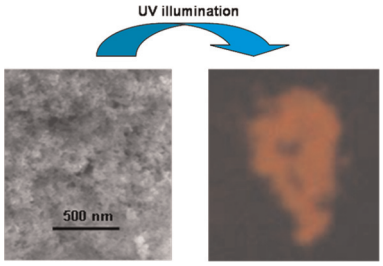

High temperature reduction of amorphous nanosilica with magnesium powder results in the formation of powder containing crystalline silicon phase The powder displays red luminescence while excited under UV illumination, due to quantum confinement within the Si nanocrystals, and can be successfully dispersed in water containing poly(vinyl alcohol) as a stabilizing agent. The obtained dispersion was also characterized by red photoluminescence, thus enabling future functional coating applications.

Synthesis and textural evolution of alumina particles with mesoporous structures
Xun Liu, Tianyou Peng, Jinchun Yao, Hongjin Lv and Cheng Huang
Page 1448

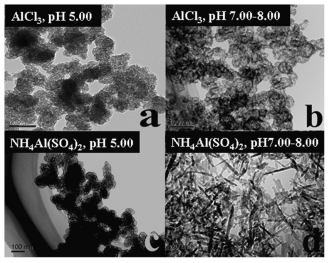

Co-existing Cl^- is beneficial for the formation of γ-alumina nanoparticles with mesostructures during the precipitation process. Interparticle and intraparticle mesopores can be derived from acidic solution and near neutral solution, respectively.

Guests inducing *p*-sulfonatocalix[4]arenes into nanocapsule and layer structure
Guoli Zheng, Weiqiang Fan, Shuyan Song, Huadong Guo and HongJie Zhang
Page 1457

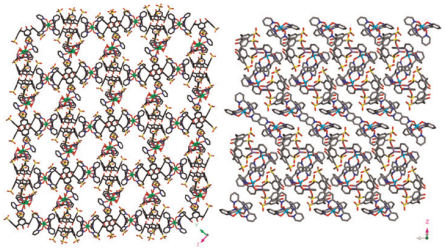

In the presence of different guests, a nanochannel architecture based on the *p*-sulfonato[4]calixarene capsule and a layered structure based on the *p*-sulfonato[4]calixarene tecton have been synthesized, and the luminescence properties and guest sorption of porous structure have been investigated.

Diversity of coordination modes in the polymers based on 3,3′,4,4′-biphenylcarboxylate ligand
Xiao-Di Du, Hong-Ping Xiao, Xin-Hui Zhou, Tao Wu and Xiao-Zeng You
Page 1464

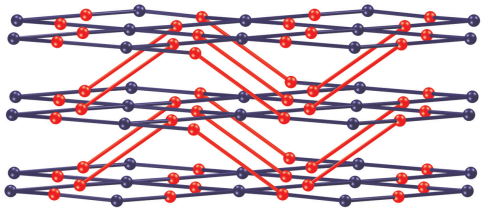

Four coordination compounds exhibiting four coordination modes of the 3,3′,4,4′-biphenylcarboxylate ligand, with three of new in this system, are obtained showing diversified architectures.

Rapid Communication

Structure and magnetic properties of $AgFeP_2O_7$
Kateryna V. Terebilenko, Alexander A. Kirichok, Vyacheslav N. Baumer, Maksym Sereduk, Nikolay S. Slobodyanik and P. Gütlich
Page 1473

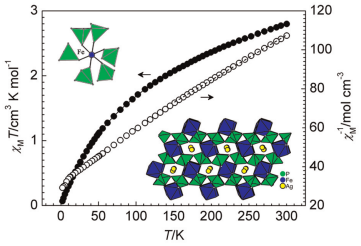

$AgFeP_2O_7$ synthesized by flux crystallization is composed of isolated iron octahedra and phosphate tetrahedra interconnected into 3D network with hexagonal channels, where silver counterions are located. The compound approaches the Curie–Weiss equation with a Weiss constant $\theta = -165.9$ K exhibiting antiferromagnetic interactions due to magnetically isolated high-spin iron(III).

Continued

Author inquiries

For inquiries relating to the submission of articles (including electronic submission where available) please visit this journal's homepage at http://www.elsevier.com/locate/jssc. You can track accepted articles at http://www.elsevier.com/trackarticle and set up e-mail alerts to inform you of when an article's status has changed. Also accessible from here is information on copyright, frequently asked questions and more.
Contact details for questions arising after acceptance of an article, especially those relating to proofs, will be provided by the publisher.

Language services. Authors who require information about language editing and copyediting services pre- and post-submission please visit http://www.elsevier.com/locate/languagepolishing or our customer support site at http://epsupport.elsevier.com. Please note Elsevier neither endorses nor takes responsibility for any products, goods or services offered by outside vendors through our services or in any advertising. For more information please refer to our Terms & Conditions http://www.elsevier.com/termsandconditions

For a full and complete Guide for Authors, please go to: http://www.elsevier.com/locate/jssc

Journal of Solid State Chemistry has no page charges.